

# A Polyanionic, Quasi-zero-strain and Open-framework $\text{K}_{0.76}\text{V}_{0.55}\text{Nb}_{0.45}\text{OPO}_4$ for Sodium-ion Batteries<sup>①</sup>

LIU Jian-Dong-Yong<sup>a, b\*</sup> YU Xu<sup>a, b\*</sup>

BAO Jing-Ze<sup>a</sup> LIN Ying-Xi<sup>a②</sup>

<sup>a</sup> (CAS Key Laboratory of Design and Assembly of Functional Nanostructures,  
and Fujian Key Laboratory of Nanomaterials, Fujian Institute of Research on the  
Structure of Matter, Chinese Academy of Sciences, Fuzhou 350002, China)

<sup>b</sup> (College of Chemistry, Fuzhou University, Fuzhou 350108, China)

**ABSTRACT** A carbon-coated  $\text{K}_{0.76}\text{V}_{0.55}\text{Nb}_{0.45}\text{OPO}_4$  (KVNP@C) polyanion material was successfully synthesized by a simple sol-gel method. The KVNP@C possesses a highly stable inorganic open-framework structure, which is hard to be affected by the  $\text{Na}^+$  intercalation/deintercalation when used as an anode material for sodium-ion batteries (NIBs). The assembled KVNP@C/Na half-cell shows a capacity retention of 81.2% and an average Coulombic efficiency of 99.8% at a current density of 300 mA/g after 1500 cycles. In-situ XRD analysis reveals a single-phase solid solution reaction mechanism with a lattice expansion of 4.76%. This work sheds insights into the quest for developing novel polyanion-based anode materials for sodium-ion batteries.

**Keywords:** anode material, sodium-ion batteries, high structural stability, solid solution reaction;

**DOI:** 10.14102/j.cnki.0254-5861.2011-3221

## 1 INTRODUCTION

At present, lithium-ion batteries (LIBs) are ubiquitous through small consumer electronics, electric vehicles, and grid-scale energy storage systems. The rapid development of LIBs has led to the continuously increasing costs of Li resources and the sharp decrease in their amount<sup>[1]</sup>. To solve this problem, alternative batteries, such as Na, K-ion batteries, have been emerging. Compared with lithium, sodium is evenly distributed and rich in reserves (the fifth most abundant element in the earth's crust), which has attracted extensive attention in recent years<sup>[2]</sup>. However, the large ionic radius of  $\text{Na}^+$  (1.02 Å) results in the large volume expansion of the anode materials during sodiation/desodiation processes, causing structural instability and rapid degradation of capacities. Therefore, developing a new type of anode material with high stability<sup>[3, 4]</sup>, long cycle life, and excellent rate performance is particularly crucial. Potential anode materials include carbon materials (hard carbon, soft carbon, etc.) and alloy compounds. However, they can hardly satisfy

the requirements of anode materials for sodium-ion batteries. For example, the low working voltage makes the hard carbon form sodium dendrites easily during the sodiation process, causing safety problems<sup>[5]</sup>; alloy materials (such as Sb,  $\text{WS}_2$  and so on) often suffer a large volume expansion, which will destroy the electrode material structure and cause serious capacity degradation<sup>[6]</sup>. Therefore, it is particularly important to develop anode materials with a safe operating voltage and a stable structure.

Polyanionic compounds, which have inorganic frameworks and high thermodynamic stability, perform well in sodium storage. The phosphate-based polyanions, such as  $\text{LiFePO}_4$ ,  $\text{LiMnPO}_4$ ,  $\text{Li}_3\text{V}_2(\text{PO}_4)_3$  and  $\text{Na}_3\text{V}_2(\text{PO}_4)_3$ , have been extensively studied and explored as electrode materials for lithium/sodium-ion batteries. Compared with other anodes, phosphate-type polyanion compounds have higher structural stabilities; and strong covalent bonds give them good thermal stability and long cycle life. In addition, the phosphate ( $\text{PO}_4^{3-}$ ) allows fast ion diffusion in an inorganic framework and stabilizes the redox potentials<sup>[7-10]</sup>. So, phosphate-type poly-

Received 15 April 2021; accepted 31 May 2021

① This project was supported by the National Natural Science Foundation of China (No. 21771180)

② Corresponding author. E-mail: linyingxi90@foxmail.com

\* These authors have contributed equally

anion compounds possess a higher operating voltage than carbon materials and can remain stable by avoiding the formation of sodium dendrites. Therefore, phosphate-type compounds have a potential as anode materials in sodium-ion batteries.

In this work, a new type of inorganic framework material carbon-coated  $\text{K}_{0.76}\text{V}_{0.55}\text{Nb}_{0.45}\text{OPO}_4$  (KVNP@C) was synthesized by a simple sol-gel method. The open framework enables reversible (de) intercalation of  $0.75 \text{ Na}^+$  per formula unit, delivering a reversible capacity of  $95.4 \text{ mAh/g}$  and capacity retention of  $75.9\%$  after 100 cycles. Even at a high current density of  $300 \text{ mA/g}$ , it still delivers a considerable capacity of  $53.5 \text{ mAh/g}$ . The in-situ XRD analysis reveals a reversible single-phase solid solution reaction with a low lattice volume expansion during the cycling.

## 2 EXPERIMENTAL

### 2.1 Preparation of KVNP@C

The carbon-coated KVNP was synthesized by a sol-gel method. First,  $2.27 \text{ g H}_2\text{C}_2\text{O}_4 \cdot 2\text{H}_2\text{O}$  and  $0.5 \text{ g H}_5\text{Nb}_3\text{O}_{10}$  were dissolved in  $10 \text{ mL}$  of deionized water, placed in an oil bath at  $76^\circ\text{C}$ , and stirred at  $400 \text{ rpm}$  for  $2 \text{ h}$  to obtain a clear solution A. Then,  $1.26 \text{ g C}_6\text{H}_8\text{O}_7 \cdot \text{H}_2\text{O}$ ,  $0.69 \text{ g NH}_4\text{H}_2\text{PO}_4$ , and  $0.39 \text{ g NH}_4\text{VO}_3$  were dissolved in  $5 \text{ mL}$  of deionized water and stirred at  $76^\circ\text{C}$  to obtain a dark blue solution B;  $0.83 \text{ g K}_2\text{CO}_3$  was dissolved in  $5 \text{ mL}$  of deionized water to obtain a clear solution C; subsequently, solution C was slowly added dropwise to solution A. When the mixed solution no longer generated bubbles, solution B was added dropwise. After mixing, the solution was stirred in an oil bath at  $76^\circ\text{C}$  at  $400 \text{ rpm}$  for  $1 \text{ h}$  to form a blue transparent solution. The formed gel was dried in an oven overnight at  $120^\circ\text{C}$ . Then the precursor was calcined at  $350^\circ\text{C}$  for  $4 \text{ h}$  and then  $900^\circ\text{C}$  for  $20 \text{ h}$  in an argon-hydrogen mixed atmosphere ( $\text{Ar:H}_2 = 95:5$ ) to obtain carbon-coated KVNP (KVNP@C).

### 2.2 Material characterization

The XRD patterns were collected on a Rigaku Ultima IV powder X-ray diffractometer ( $\text{CuK}\alpha$  radiation). The microscopic morphology of the material was characterized by a scanning electron microscope (SEM, Hitachi SU-8010) and transmission electron microscope (TEM, FEI Tecnai G2 F20). The energy-dispersive X-ray spectroscopy (EDS) was used to characterize the elemental composition and distribution of KVNP@C. Inductively Coupled Plasma (ICP, JY Ultima-2) was used to determine the content in KVNP@C.

### 2.3 Preparation of working electrode

The active material (KVNP@C), conductive carbon black (Super P Carbon), and carboxymethylcellulose (CMC) binder were mixed at a weight ratio of  $8:1:1$  and then stirred at  $800 \text{ rpm}$  for  $12 \text{ h}$  to obtain a uniform black slurry. Then, the black slurry was evenly coated on aluminum foil and placed in a vacuum oven at  $100^\circ\text{C}$  for  $12 \text{ h}$ . The mass loading of the KVNP@C electrode is about  $1.4 \text{ mg/cm}^2$ .

### 2.4 Half-cell assembly

The coin-type cells (CR2032) were used to assemble half-cells in a glove box filled with high-purity argon (both water content and oxygen content are less than  $0.1 \text{ ppm}$ ). The electrolyte was  $1 \text{ M NaClO}_4$  in EC/DEC with  $10\% \text{ FEC}$ . The in-situ battery used a self-made battery device.

### 2.5 Electrochemical measurements

Galvanostatic cycling tests and rate performance tests were carried out on LAND-CT2011A battery-testing instruments under room temperature, where the voltage range was from  $0.1$  to  $2.2 \text{ V}$  (vs  $\text{Na/Na}^+$ ). Cyclic voltammetry (CV) was measured on a CHI660E electrochemical workstation (Shanghai Chenhua, China) with a voltage range of  $0.1\sim 2.2 \text{ V}$  (vs.  $\text{Na/Na}^+$ ). Rate-scan CV was performed on a Bio-Logic SP-300 electrochemical workstation with scan rates from  $0.02$  to  $0.15 \text{ mV/s}$ .

### 2.6 In-situ XRD test

An in-situ battery was made with a beryllium window capable of penetrating XRD rays, and a galvanostatic charge and discharge test at  $10 \text{ mA/g}$  was performed on LAND-CT2011A battery-testing instruments. In the meantime, XRD signals were continuously collected at a scanning rate of  $5^\circ/\text{minute}$  by Rigaku Ultima IV powder XRD with  $\text{CuK}\alpha$  radiation at a voltage of  $40 \text{ kV}$  and a current of  $40 \text{ mA}$ .

## 3 RESULTS AND DISCUSSION

As illustrated in Fig. 1a, the KVNP@C is composed of  $\text{NbO}_6/\text{VO}_6$  octahedra and  $\text{PO}_4$  tetrahedra with K-ions filled in the open channels, showing a typical  $\text{KTiOPO}_4$  (KTP) structure<sup>[11]</sup>. Besides, the elements of Nb prefer to occupy the center of octahedra, while the V occupies the center of the residual octahedra. The  $\text{VO}_6$  octahedron is more regular than  $\text{NbO}_6$ <sup>[12]</sup>, reducing the whole distortion degree of octahedra, which would greatly reduce the possibility of lattice deformation during the intercalation of sodium ions. Fig. 1b shows the results of X-ray powder diffraction (XRD) Rietveld refined of KVNP@C ( $R_{\text{wp}} = 6.87\%$ ,  $R_p = 4.96\%$ ). It can be seen that all

the diffraction peaks are consistent with the theoretical values and indexed in an orthorhombic system. The unit cell parameters obtained by the refined structure are  $a = 12.93$ ,  $b = 6.47$  and  $c = 10.73$  Å, respectively. The inductively coupled plasma emission spectroscopy (ICP-OES) result gave a K:V:Nb molar ratio of 0.76:0.55:0.45, so the chemical formula can be determined as  $K_{0.76}V_{0.55}Nb_{0.45}OPO_4$ . Due to the low potassium content in KVNP@C, a large number of

vacancies and open channels are expected to host sodium-ions without damaging the structure. The SEM image (Fig. 1c) of KVNP@C exhibits a uniform particle size of about 500 nm. And, the high-resolution TEM (HRTEM) image of KVNP@C shows a well-covered (the carbon layer is about 2 nm) KVNP with a lattice space of 0.56 nm, indexing to the (201) lattice plane (Fig. 1d). Furthermore, TEM-EDS mapping proves that various elements in the sample are uniformly distributed (Fig. 1e).

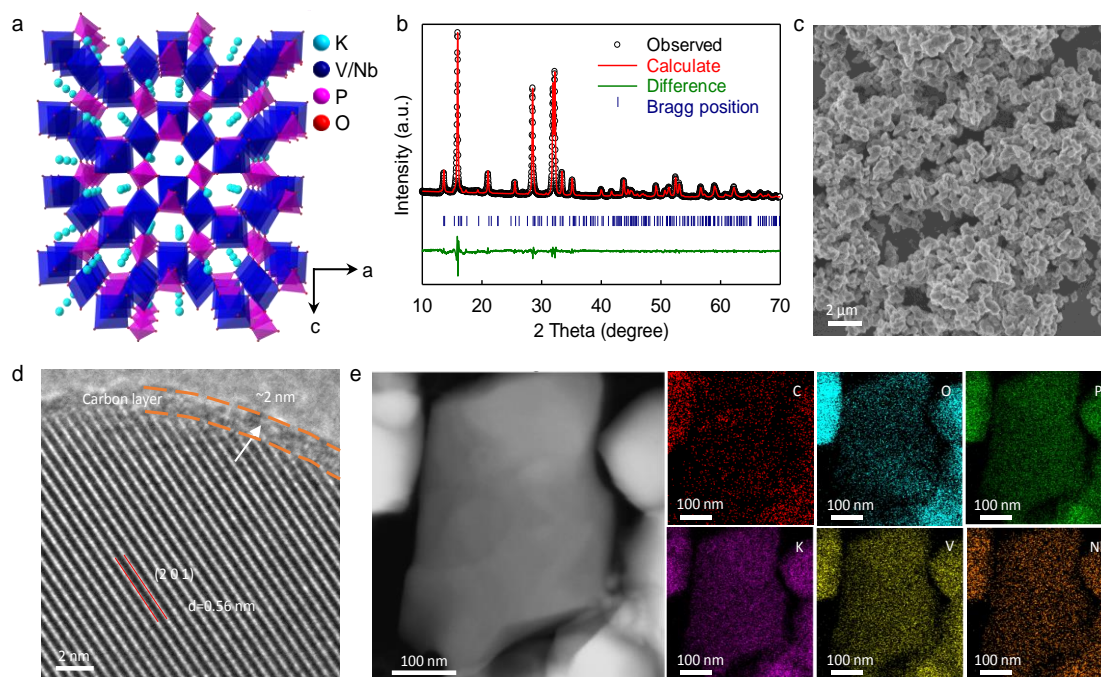
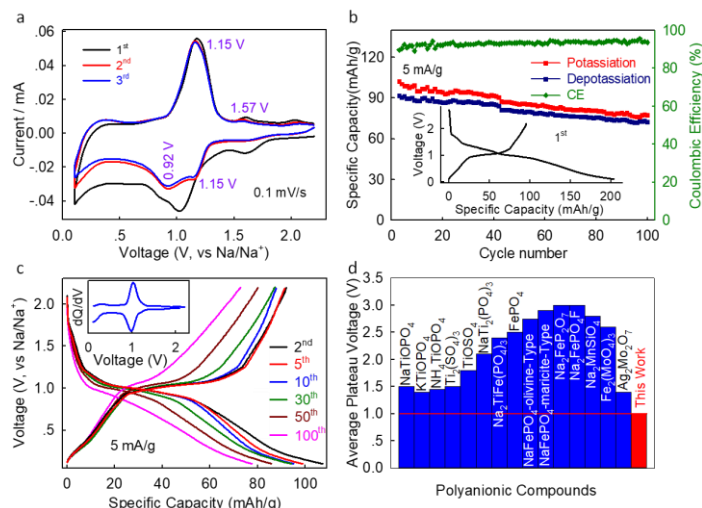


Fig. 1. (a) Crystal structure diagram of KVNP; (b) XRD Rietveld refinement of KVNP@C (Rwp = 6.87%, Rp = 4.96%); (c) SEM image of KVNP@C; (d) TEM image of KVNP@C; (e) EDS element distribution image of KVNP@C

Fig. 2a presents the initial three cycles of cyclic voltammetry (CV) profiles at a scan rate of 0.1 mV/s. The reduction peak of the first cycle between 0.9 and 1.1 V (vs Na/Na<sup>+</sup>) corresponds to the intercalation of Na<sup>+</sup> and the formation of solid electrolyte interface (SEI). The oxidation peaks at around 1.15 and 1.57 V correspond to the extraction of sodium ions. After the initial cycle, the CV curves of the following two circles almost overlap, indicating a highly reversible process. The inset in Fig. 2b is the first cycle voltage profile of KVNP@C/Na half-cells at a current density of 5 mA/g (rate of ~0.05 C), the reversible specific capacity of KVNP@C is 95.4 mAh/g (the volume energy density is 312.9 mAh/cm<sup>3</sup>), implying a 0.75 sodium-ion intercalation in each KVNP@C molecule (calculated based on the theoretical specific capacity). The initial Coulombic efficiency (CE) of 46.8% is mainly attributed to the formation of irreversible SEIs, which is common for anodes in sodium-ion batteries<sup>[13]</sup>.

Even at such a low current density (5 mA/g), KVNP@C still exhibits a reversible specific capacity of 72.4 mAh/g after 100 cycles, remaining 75.9% of the initial capacity. The charge and discharge curves during the cycle are shown in Fig. 2c. The voltage profiles and the inset of the fifth dQ/dV curve indicate a voltage plateau of 0.99 V for the insertion of Na<sup>+</sup> and a voltage of 1.05 V for the deintercalation of Na<sup>+</sup> progress. The dQ/dV curve also shows a narrow polarization voltage for only 0.06 V. The voltage plateau can always be observed in the charge and discharge curves of different cycles, which is consistent with the CV profiles, indicating that KVNP@C can maintain a stable structure during the extraction/intercalation process. Compared with other polyanion anodes<sup>[14-26]</sup>, KVNP@C has the lowest operating voltage (0.99 V), which is beneficial to achieve a higher energy density for the full-cell application.



**Fig. 2.** (a) CV profiles of the KVNP@C electrode at a scan rate of 0.1 mV/s; (b) Galvanostatic cycling of the KVNP@C electrode at a current of 5 mA/g. The inset shows the voltage profile of the first cycle; (c) Voltage profiles of the KVNP@C electrode at a current of 5 mA/g. The inset is the corresponding dQ/dV curve at the fifth cycle; (d) Comparison of average platform voltages of polyanionic compounds

Fig. 3 displays the long-cycling performance of KNVP@C, which was tested at current densities of 100 and 300 mA/g followed by two-cycles of activation at 5 mA/g. The KNVP@C delivers a reversible capacity of 79.9 mAh/g at 100 mA/g with a CE of 97.5%. After 1000 charge/discharge cycles, a capacity of 82.5% can be retained. Moreover, KNVP@C achieves a capacity of 53.5 mAh/g at the high rate of 300

mA/g, and the capacity increases to 66.1 mAh/g at the 296<sup>th</sup> cycle. The final capacity retention is 81.2% and an average CE of 99.8% can be achieved after 1500 cycles. The above results exhibit the excellent cycling stability of KNVP@C, attributed to the reducing structural distortion benefiting from Nb/V co-doping.

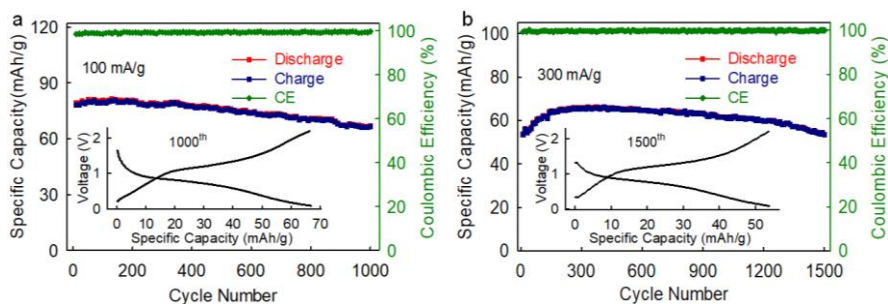


**Fig. 3.** (a, b) Electrochemical cycle performance of KVNP@C at current densities of 100 and 300 mA·g<sup>-1</sup>, respectively; Insets in (a) and (b) are the corresponding voltage profiles, respectively

As shown in Fig. 4, rate CV was performed to investigate the Na<sup>+</sup> storage kinetics of KVNP@C electrodes. The scanning voltage window and the scan rates were selected in a range of 0.1~2.2 V (vs Na/Na<sup>+</sup>) and from 0.02 to 0.15 mV/s, respectively. With the increase of scanning rate, the oxidation peak gradually shifts to the high voltage position, and the reduction peak shifts to the opposite direction. It shows that the faster scanning rates will affect the electrochemical oxidation-reduction process and cause electrochemical polarization. Then, we calculated the Na<sup>+</sup> diffusion coefficients of KVNP@C electrodes by the Randles-Sevcik

equation. To qualitatively analyze the contribution of diffusion and surface-induced capacitance, the functional relationship (Equation 1) between current (*i*) and scan rate (*v*) is shown as follows, where *a* and *b* are the adjustment constants.

$$i = av^b \quad (\text{equation 1})^{[27]}$$

Generally, the value of *b* varies between 0.5 and 1.0. When the value of *b* is around 0.5, it indicates the electrochemical process controlled by diffusion behavior<sup>[28-30]</sup>; while the *b*-value of 1 refers to a surface-induced behavior, i.e. pseudocapacitance. Herein, the value of *b* is determined by

slope of  $\log(i)$  and  $\log(v)$  obtained from CV curves (Fig. 4b), which shows values of 0.86 and 0.75 for peaks 1 and 2, respectively<sup>[31, 32]</sup>. It indicates that the electrochemical process

of KVNP@C is partly controlled by capacitive behavior, resulting in the fast sodium-ion reaction kinetics.

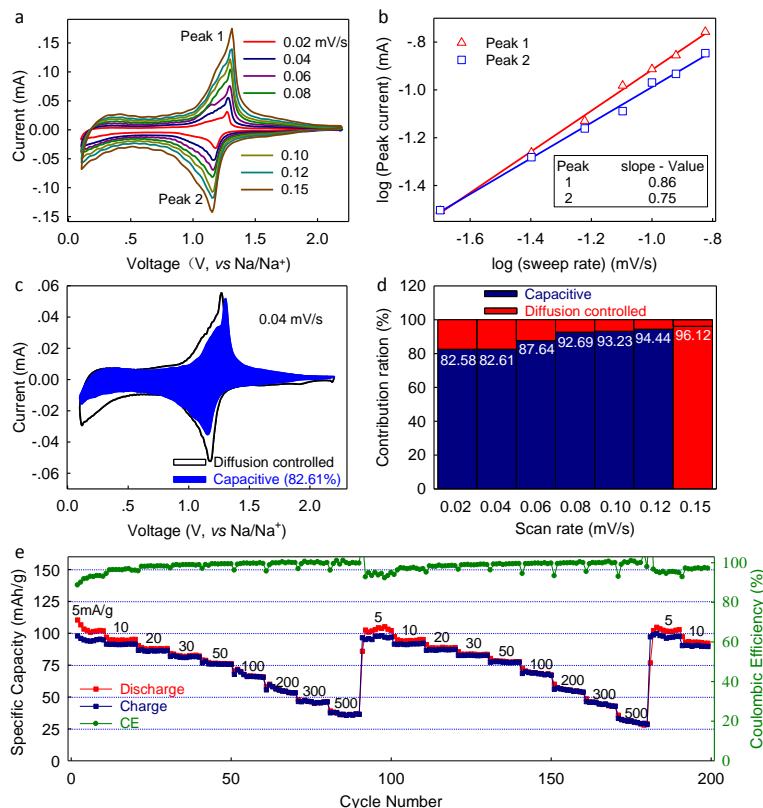


Fig. 4. (a) CV curves at various scan rates, (b) Fitting line of  $\log(\text{sweep rate, mV/s})$  vs.  $\log(I_{\text{peak, mA}})$  of KVNP@C, (c) capacitive contributions at 0.04 mV/s, (d) Ratio of capacitive contribution at various scan rates, (e) Rate capability

In detail, the contributions of capacitive and diffusion can be calculated based on equation 2:

$$i(V) = k_1 v + k_2 v^{1/2} \quad (\text{equation 2})$$

where  $k_1 v$  and  $k_2 v^{1/2}$  represent surface capacitive and diffusion control processes, respectively. Fig. 4c presents the pseudocapacitance contribution of the KVNP@C electrode at a scan rate of 0.04 mV/s, in which the proportion is about 82.61%. The proportion of pseudocapacitance increases as the scan rate increases, which grows from 82.58% to 96.12%. The calculated results imply that the inorganic framework of KVNP@C can possess abundant pathways for the  $\text{Na}^+$  going through electrodes and electrolytes, leading to fast charge transfer for a better rate performance.

Additionally, the rate performance is investigated at different current densities ranging from 5 to 500 mA/g (Fig. 4e). The KVNP@C/Na battery delivers charging capacity of 95.8, 91.6, 86.9, 82.6, 77.8, 69.2, 56.4, and 46.0 mAh/g at 5, 10, 20, 30, 50, 100, 200, 300 and 500 mA/g, respectively. After two repeated rate cycles, the charge capacity still maintains 90.5 mAh/g when going back to the initial current

density. Based on the above analysis, it can be shown that the KVNP@C anode boasts an excellent rate performance and long-cycle stability.

To verify the structural evolution of the KVNP@C electrode during the intercalation/deintercalation of  $\text{Na}^+$ , in-situ XRD technology was conducted (Fig. 5a and b). Three obvious peaks changed during  $\text{Na}^+$  (de)intercalation, which can be assigned to (201), (203), and (022) Bragg peaks. During the entire discharging process, all three peaks shift slightly toward a lower angle and there are no additional peaks emerging, which means the formation of solid solution in the compound. The charge follows the same but inverse peaks shifting, revealing a highly reversible phase change process. Fig. 5b shows the diffraction patterns at different states of charge. The lattice parameters obtained from Rietveld refinement have been summarized in Fig. 5e. The selected calculated results (Fig. 5d and f) show that the lattice constants  $a$ ,  $b$ , and  $c$  increase from 12.86, 6.44, and 10.71 Å to 13.04, 6.50, and 10.98 Å, respectively ( $R_{\text{wp}}$  and  $R_p$  are 4.89%, 4.74%, and 2.26%, 2.23%, respectively). Consequently,

despite the large size of  $Na^+$ , the total volume difference between the original sample and fully discharged KVNP@C is only 4.76% (Fig. 5e), which is less than those of alloybased compounds ( $Sn_4P_3$ , Sb, Sn, P) and metal oxides ( $SnO_2$ ,  $Fe_2O_3$ )<sup>[33-38]</sup>. Compared with reported polyanionic materials in sodium ion batteries, KVNP@C shows the most minimal

volume expansion (Fig. S1), revealing the superiority of its structure. Based on the above experimental results, we confirm that the small volume change is the key point that enables the great cycling stability of KVNP@C as a novel promising candidate anode for next-generation NIBs.

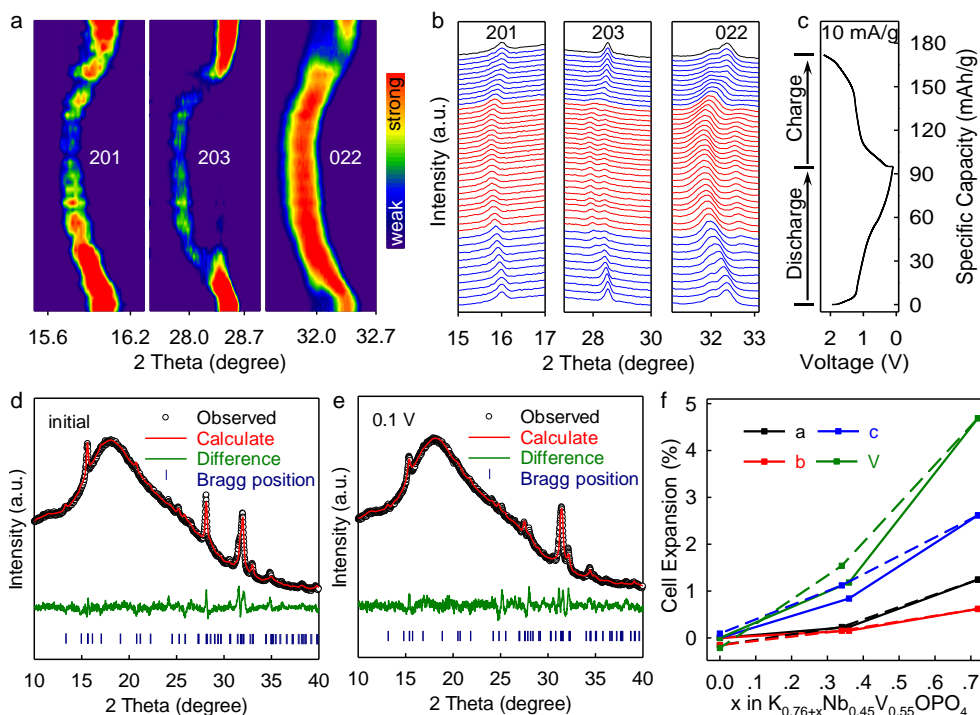


**Fig. 5.** (a) Contour plot and (b) line patterns of in-situ XRD patterns of the KVNP@C electrode with a different state of charge, and (c) the corresponding charge-discharge profile of the electrode, (d) XRD pattern and the corresponding Rietveld refinement of the initial KVNP@C, and (e) the sodiated KVNP@C, (f) Lattice-constant evolution upon cycling. Solid and dashed lines represent the discharging and charging process, respectively

## 4 CONCLUSION

In summary, a new type of negative electrode material KVNP@C for sodium-ion batteries was successfully prepared by a simple sol-gel method. Electrochemical research results show that KVNP@C has excellent cycle stability and good rate performance. Under low current density discharge (5 mA/g), the capacity retention rate of KVNP@C is 75.9% after 100 cycles. Even at a high current density of 300 mA/g ( $\approx 3$  C), the capacity retention rate and average Coulombic efficiency are 81.2% and 99.8% after 1500 cycles, respec-

tively, indicating that the material has high reversibility of electrochemical sodium (de)intercalation. Kinetic mechanisms show that KVNP@C as an anode material has a rapid sodium-ion transfer rate. Moreover, the in-situ XRD analysis verified that the sodium-ion intercalation process of KVNP@C is a single-phase solid solution reaction with a lattice volume expansion of merely 4.76%. Based on the above analysis, KVNP@C material has high structural stability and good electrochemical performance, which has a potential to be applied to the anodes of next-generation sodium-ion batteries.

## REFERENCES

- (1) Muñoz-Márquez, M. Á.; Saurel, D.; Gámez-Cámer, J. L.; Casas-Cabanas, M.; Castillo-Martínez, E.; Rojo, T. Na-ion batteries for large scale applications: a review on anode materials and solid electrolyte interphase formation. *Adv. Energy Mater.* **2017**, 7, 1700463.
- (2) Kim, J.; Choi, M. S.; Shin, K. H.; Kota, M.; Kang, Y.; Lee, S.; Lee, J. Y.; Park, H. S. Rational design of carbon nanomaterials for electrochemical sodium storage and capture. *Adv. Mater.* **2019**, 31, 1803444.



- (3) Ong, S. P.; Chevrier, V. L.; Hautier, G.; Jain, A.; Moore, C.; Kim, S.; Ma, X.; Ceder, G. Voltage, stability and diffusion barrier differences between sodium-ion and lithium-ion intercalation materials. *Energy Environ. Sci.* **2011**, 4, 3680–3688.
- (4) Sun, Y.; Guo, S.; Zhou, H. Exploration of advanced electrode materials for rechargeable sodium-ion batteries. *Adv. Energy Mater.* **2018**, 9, 1800212.
- (5) Cao, Y.; Xiao, L.; Sushko, M. L.; Wang, W.; Schwenzer, B.; Xiao, J.; Nie, Z.; Saraf, L. V.; Yang, Z.; Liu, J. Sodium ion insertion in hollow carbon nanowires for battery applications. *Nano Lett.* **2012**, 12, 3783–3787.
- (6) Wang, G. Z.; Feng, J. M.; Dong, L.; Li, X. F.; Li, D. J. Porous graphene anchored with Sb/sbox as sodium-ion battery anode with enhanced reversible capacity and cycle performance. *J. Alloys Compd.* **2017**, 693, 141–149.
- (7) Tamaru, M.; Chung, S. C.; Shimizu, D.; Nishimura, S. I.; Yamada, A. Pyrophosphate chemistry toward safe rechargeable batteries. *Chem. Mater.* **2013**, 25, 2538–2543.
- (8) Ellis, B. L.; Lee, K. T.; Nazar, L. F. Positive electrode materials for Li-ion and Li-batteries. *Chem. Mater.* **2010**, 22, 691–714.
- (9) Palomares, V.; Serras, P.; Villaluenga, I.; Hueso, K. B.; Carretero-González, J.; Rojo, T. Na-ion batteries, recent advances and present challenges to become low cost energy storage systems. *Energy Environ. Sci.* **2012**, 5, 5884–5901.
- (10) Zhu, C.; Song, K.; van Aken, P. A.; Maier, J.; Yu, Y. Carbon-coated  $\text{Na}_3\text{V}_2(\text{PO}_4)_3$  embedded in porous carbon matrix: an ultrafast Na-storage cathode with the potential of outperforming Li cathodes. *Nano Lett.* **2014**, 14, 2175–2180.
- (11) Bierlein, J. D.; Vanherzeele, H. Potassium titanyl phosphate-properties and new applications. *J. Opt. Soc. AM. B* **1989**, 6, 622–633.
- (12) Rangan, K. K.; Verbaere, A.; Gopalakrishnan, J. Structure of  $\text{KNb}_{0.5}\text{V}_{0.5}\text{OPO}_4$ , a  $\text{KTiOPO}_4$  analog. *Mater. Res. Bull.* **1998**, 33, 395–399.
- (13) Bommier, C.; Ji, X. Electrolytes, sei formation, and binders: a review of nonelectrode factors for sodium-ion battery anodes. *Small.* **2018**, 14, 1703576.
- (14) Kim, J.; Seo, D. H.; Kim, H.; Park, I.; Yoo, J. K.; Jung, S. K.; Park, Y. U.; Goddard Iii, W. A.; Kang, K. Unexpected discovery of low-cost maricite  $\text{NaFePO}_4$  as a high-performance electrode for Na-ion batteries. *Energy Environ. Sci.* **2015**, 8, 540–545.
- (15) Liu, Y.; Xu, Y.; Han, X.; Pellegrinelli, C.; Zhu, Y.; Zhu, H.; Wan, J.; Chung, A. C.; Vaaland, O.; Wang, C.; Hu, L. Porous amorphous  $\text{FePO}_4$  nanoparticles connected by single-wall carbon nanotubes for sodium ion battery cathodes. *Nano Lett.* **2012**, 12, 5664–5668.
- (16) Sun, Q.; Ren, Q. Q.; Fu, Z. W. Nasicon-type  $\text{Fe}_2(\text{MoO}_4)_3$  thin film as cathode for rechargeable sodium ion battery. *Electrochem. Commun.* **2012**, 23, 145–148.
- (17) Tripathi, R.; Wood, S. M.; Islam, M. S.; Nazar, L. F. Na-ion mobility in layered  $\text{Na}_2\text{FePO}_4\text{F}$  and olivine  $\text{Na}[\text{Fe}, \text{Mn}]\text{PO}_4$ . *Energy Environ. Sci.* **2013**, 6, 2257–2264.
- (18) Chen, C. Y.; Matsumoto, K.; Nohira, T.; Hagiwara, R.  $\text{Na}_2\text{MnSiO}_4$  as a positive electrode material for sodium secondary batteries using an ionic liquid electrolyte. *Electrochem. Commun.* **2014**, 45, 63–66.
- (19) Kim, H.; Shakoar, R. A.; Park, C.; Lim, S. Y.; Kim, J. S.; Jo, Y. N.; Cho, W.; Miyasaka, K.; Kahraman, R.; Jung, Y.; Choi, J. W.  $\text{Na}_2\text{FeP}_2\text{O}_7$  as a promising iron-based pyrophosphate cathode for sodium rechargeable batteries: a combined experimental and theoretical study. *Adv. Funct. Mater.* **2013**, 23, 1147–1155.
- (20) Fang, Y.; Liu, Q.; Xiao, L.; Ai, X.; Yang, H.; Cao, Y. High-performance olivine  $\text{NaFePO}_4$  microsphere cathode synthesized by aqueous electrochemical displacement method for sodium ion batteries. *ACS Appl. Mater. Interfaces* **2015**, 7, 17977–17984.
- (21) Yang, J.; Wang, H.; Hu, P.; Qi, J.; Guo, L.; Wang, L. A high-rate and ultralong-life sodium-ion battery based on  $\text{NaTi}_2(\text{PO}_4)_3$  nanocubes with synergistic coating of carbon and rutile  $\text{TiO}_2$ . *Small.* **2015**, 11, 3744–3749.
- (22) Patoux, S.; Rousse, G.; Leriche, J. B.; Masquelier, C. Structural and electrochemical studies of rhombohedral  $\text{Na}_2\text{TiM}(\text{PO}_4)_3$  and  $\text{Li}_{1.6}\text{Na}_{0.4}\text{TiM}(\text{PO}_4)_3$  (M: Fe, Cr) phosphates. *Chem. Mater.* **2003**, 15, 2084–2093.
- (23) Chen, N.; Gao, Y.; Zhang, M.; Meng, X.; Wang, C.; Wei, Y.; Du, F.; Chen, G. Electrochemical properties and sodium-storage mechanism of  $\text{Ag}_2\text{Mo}_2\text{O}_7$  as the anode material for sodium-ion batteries. *Chem-Eur. J.* **2016**, 22, 7248–7254.
- (24) Gnanavel, M.; Raveau, B.; Pralong, V. Electrochemical Li/Na intercalation in  $\text{TiOSO}_4$ , first member of the phosphate tungsten bronze-type family. *J. Electrochem. Soc.* **2015**, 162, A465–A469.
- (25) Senguttuvan, P.; Rousse, G.; Vezin, H.; Tarascon, J. M.; Palacin, M. R. Titanium(III) sulfate as new negative electrode for sodium-ion batteries. *Chem. Mater.* **2013**, 25, 2391–2393.
- (26) Mu, L.; Ben, L.; Hu, Y. S.; Li, H.; Chen, L.; Huang, X. Novel 1.5 V anode materials,  $\text{ATiOPO}_4$  (A =  $\text{NH}_4$ , K, Na), for room-temperature sodium-ion batteries. *J. Mater. Chem. A* **2016**, 4, 7141–7147.
- (27) Chen, C.; Wen, Y.; Hu, X.; Ji, X.; Yan, M.; Mai, L.; Hu, P.; Shan, B.; Huang, Y.  $\text{Na}^+$  intercalation pseudocapacitance in graphene-coupled titanium

- oxide enabling ultra-fast sodium storage and long-term cycling. *Nat. Commun.* **2015**, 6, 1–8.
- (28) Zhao, G.; Zhang, Y.; Yang, L.; Jiang, Y.; Zhang, Y.; Hong, W.; Tian, Y.; Zhao, H.; Hu, J.; Zhou, L.; Hou, H.; Ji, X.; Mai, L. Nickel chelate derived  $NiS_2$  decorated with bifunctional carbon: an efficient strategy to promote sodium storage performance. *Adv. Funct. Mater.* **2018**, 28, 1803690.
- (29) Zou, G.; Hou, H.; Foster, C. W.; Banks, C. E.; Guo, T.; Jiang, Y.; Zhang, Y.; Ji, X. Advanced hierarchical vesicular carbon co-doped with S, P, N for high-rate sodium storage. *Adv. Sci.* **2018**, 5, 1800241.
- (30) Lindström, H.; Södergren, S.; Solbrand, A.; Rensmo, H.; Hjelm, J.; Hagfeldt, A.; Lindquist, S. E.  $Li^+$  ion insertion in  $TiO_2$  (anatase). 2. Voltammetry on nanoporous films. *J. Phys. Chem. B* **1997**, 101, 7717–7722.
- (31) Augustyn, V.; Come, J.; Lowe, M. A.; Kim, J. W.; Taberna, P. L.; Tolbert, S. H.; Abruña, H. D.; Simon, P.; Dunn, B. High-rate electrochemical energy storage through  $Li^+$  intercalation pseudocapacitance. *Nat. Mater.* **2013**, 12, 518–522.
- (32) Xiao, Y.; Wang, P. F.; Yin, Y. X.; Zhu, Y. F.; Niu, Y. B.; Zhang, X. D.; Zhang, J.; Yu, X.; Guo, X. D.; Zhong, B. H.; Guo, Y. G. Exposing active facets by multiple-layer oriented stacking nanosheets for high-performance capacitive sodium-ion oxide cathode. *Adv. Mater.* **2018**, 30, 1803765.
- (33) Gu, M.; Kushima, A.; Shao, Y.; Zhang, J. G.; Liu, J.; Browning, N. D.; Li, J.; Wang, C. Probing the failure mechanism of  $SnO_2$  nanowires for sodium-ion batteries. *Nano Lett.* **2013**, 13, 5203–5211.
- (34) Liu, Y.; Zhang, N.; Jiao, L.; Chen, J. Tin nanodots encapsulated in porous nitrogen-doped carbon nanofibers as a free-standing anode for advanced sodium-ion batteries. *Adv. Mater.* **2015**, 27, 6702–6707.
- (35) Liu, J.; Kopold, P.; Wu, C.; van Aken, P. A.; Maier, J.; Yu, Y. Uniform yolk-shell  $Sn_4P_3@C$  nanospheres as high-capacity and cycle-stable anode materials for sodium-ion batteries. *Energy Environ. Sci.* **2015**, 8, 3531–3538.
- (36) Liang, L.; Xu, Y.; Wang, C.; Wen, L.; Fang, Y.; Mi, Y.; Zhou, M.; Zhao, H.; Lei, Y. Large-scale highly ordered sb nanorod array anodes with high capacity and rate capability for sodium-ion batteries. *Energy Environ. Sci.* **2015**, 8, 2954–2962.
- (37) Zhang, N.; Han, X.; Liu, Y.; Hu, X.; Zhao, Q.; Chen, J. 3D porous  $\gamma\text{-Fe}_2O_3@C$  nanocomposite as high-performance anode material of Na-ion batteries. *Adv. Energy Mater.* **2015**, 5, 1401123.
- (38) Sun, J.; Lee, H. W.; Pasta, M.; Yuan, H.; Zheng, G.; Sun, Y.; Li, Y.; Cui, Y. A phosphorene-graphene hybrid material as a high-capacity anode for sodium-ion batteries. *Nat. Nanotechnol.* **2015**, 10, 980–985.